Yinsheng Li
Japan Atomic Energy Agency,
Tokai-mura, Naka-gun,
Ibaraki-ken 319-1195, Japan
e-mail: li.yinsheng@jaea.go.jp

Kunio Hasegawa
Japan Atomic Energy Agency,
Tokai-mura, Naka-gun,
Ibaraki-ken 319-1195, Japan
e-mail: hasegawa.kunio@jaea.go.jp

Genshichiro Katsumata
Japan Atomic Energy Agency,
Tokai-mura, Naka-gun,
Ibaraki-ken 319-1195, Japan
e-mail: katsumata.genshichiro@jaea.go.jp

Kazuya Osakabe
Mizuho Information and Research Institute,
2-3 Kanda-Nishikicho, Chiyoda-ku,
Tokyo 101-8443, Japan
e-mail: kazuya.osakabe@mizuho-ir.co.jp

Hiroshi Okada
Tokyo University of Science,
2641 Yamazaki, Noda,
Chiba 278-8510, Japan
e-mail: hokada@rs.noda.tus.ac.jp

Development of Stress Intensity Factors for Surface Cracks With Large Aspect Ratio in Plates

A number of surface cracks with large aspect ratio have been detected in components of nuclear power plants (NPPs) in recent years. The depths of these cracks are even larger than the half of crack lengths. When a crack is detected during in-service inspections, methods provided in ASME Boiler and Pressure Vessel Code Section XI or JSME Rules on fitness-for-service for NPPs can be used to assess the structural integrity of cracked components. The solution of the stress intensity factor (SIF) is very important in the structural integrity assessment. However, in the current codes, the solutions of the SIF are provided for semi-elliptical surface cracks with a limitation of $a/\ell \leq 0.5$, where a is the crack depth, and ℓ is the crack length. In this study, the solutions of the SIF were calculated using finite element analysis (FEA) with quadratic hexahedron elements for semi-elliptical surface cracks with large aspect ratio in plates. The crack dimensions were focused on the range of $a/\ell = 0.5$–4.0 and $a/t = 0.0$–0.8, where t is the wall thickness. Solutions were provided at both the deepest and the surface points of the surface cracks. Furthermore, some of solutions were compared with the available existing results as well as with solutions obtained using FEA with quadratic tetrahedral elements and the virtual crack closure-integral method (VCCM). Finally, it was concluded that the solutions proposed in this paper are applicable in engineering applications.
[DOI: 10.1115/1.4030026]

Keywords: stress intensity factor, semi-elliptical surface crack, crack with large aspect ratio, stress corrosion cracking, finite element analysis, fitness-for-service

1 Introduction

In recent years, a number of surface cracks with large aspect ratio were detected in components of NPPs, for example, the crack detected in the weld of reactor vessel nozzle at Ohi Unit-3 PWR plant [1], the crack found in the weld of the pressurizer safety and relief nozzle at Tsuruga Unit-2 PWR plant [1], and the crack detected in the weld of the shroud support at Tsuruga Unit-1 BWR plant [2]. These cracks were caused by stress corrosion cracking (SCC). The crack depths were even larger than the half-lengths.

When a crack is detected in components during in-service inspections, structural integrity assessment usually has to be conducted taking crack growth and failure evaluation into account. ASME Boiler and Pressure Vessel Code Section XI (ASME Section XI) [3] and JSME rules on fitness-for-service for NPPs (JSME FFS Code) [4] provide flaw evaluation procedures for integrity assessment. The SIF is a highly important mechanical parameter in structural integrity assessment of cracked components. Many SIF solutions have been proposed and included in codes such as the ASME Section XI, the JSME FFS Code, API 579-1/ASME FFS-1 [5], or RSE-M [6]. However, in these current codes, the applicable ranges of the provided SIF solutions are limited. For example, the ASME Section XI and the JSME FFS Code provide SIF solutions within $a/\ell \leq 0.5$, where a is the crack depth, ℓ is the total crack length, and a/ℓ is called aspect ratio, as shown in Fig. 1. Although this limitation may be rational for fatigue cracks, it may not be useful for cracks due to SCC because SCC may induce cracks with large aspect ratios [7]. Therefore, it is important to provide SIF solutions for semi-elliptical surface cracks with large aspect ratio of $a/\ell > 0.5$. The Working Groups on Pipe Flaw Evaluation and Flaw Evaluation of the ASME Section XI are developing the SIF solutions for semi-elliptical surface cracks with large aspect ratio and this paper is a part of the work in the working groups.

Malekian et al. [8] calculated the SIF solutions for semi-elliptical surface cracks in flat plates with a/ℓ to 4.0 using FEA and extended FEA. Although SIF detailed solutions were not provided in their paper, some important features were reported, for instance, for semi-elliptical surface cracks with $a/\ell \geq 1.0$, the maximum SIF solution may be found between the surface point and the deepest point for some specific stress distributions acting on the crack surface. Iwamatsu et al. [9] calculated the SIF solutions for semi-elliptical surface cracks in flat plates with a/ℓ to 2.5. In their calculations, instead of the influence functions for polynomial stress distribution, which is used in many fitness-for-service codes, a database with a large number of influence coefficients corresponding to the unit force at every node of the finite elements, which is used to represent the crack surface in FEA, was established. The characteristic feature of their method is that the SIF solution can be calculated for any arbitrary stress distribution, based on the influence coefficient database. Ochi et al. [10] also calculated the SIF solutions, including solutions for surface cracks with large aspect ratio. Although the crack shape was characterized as rectangular instead of semi-elliptical, the detailed SIF solutions were provided at the deepest point for axial cracks in cylinders.

In this study, SIF solutions were calculated for semi-elliptical surface cracks with large aspect ratio in plates using FEA with quadratic hexahedron elements. The crack shape was characterized as a semi-elliptical surface crack. The stress distribution at the crack location was represented as a fourth-order polynomial

Contributed by the Pressure Vessel and Piping Division of ASME for publication in the JOURNAL OF PRESSURE VESSEL TECHNOLOGY. Manuscript received November 5, 2014; final manuscript received March 7, 2015; published online June 16, 2015. Assoc. Editor: David L. Rudland.

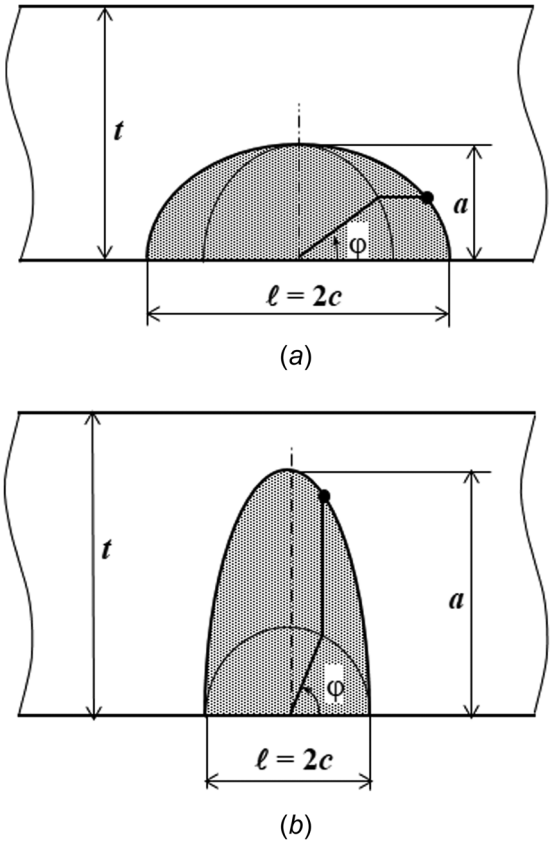

Fig. 1 Geometries of surface semi-elliptical crack in a plate. (*a*) Surface semi-elliptical crack with $a/\ell \le 0.5$ and (*b*) surface semi-elliptical crack with $a/\ell > 0.5$.

equation. The crack dimensions were focused on the range of $a/\ell = 0.5$ to 4.0 and $a/t = 0.0$ to 0.8, where t is the wall thickness. Influence function solutions were provided for both the deepest and the surface points of the cracks. A number of solutions were compared with the available existing solutions to confirm the applicability. Furthermore, the solutions were also compared with solutions obtained using the VCCM [11] with quadratic tetrahedral elements [12].

2 Applicable Ranges of SIF for Semi-Elliptical Surface Cracks in Current Codes

As mentioned above, many SIF solutions have been provided in current codes [3–6]. The applicable ranges of the provided solutions considering polynomial stress distribution are summarized in Table 1 for semi-elliptical surface cracks in plates. It can be seen from this table that the applicable ranges of the provided solutions are limited within $a/\ell \le 0.5$.

It is well known that surface cracks with deep depth and short length of $a/\ell > 0.5$ will approach to a semi-circle crack of $a/\ell = 0.5$ under cyclic tensile loading for fatigue crack growth.

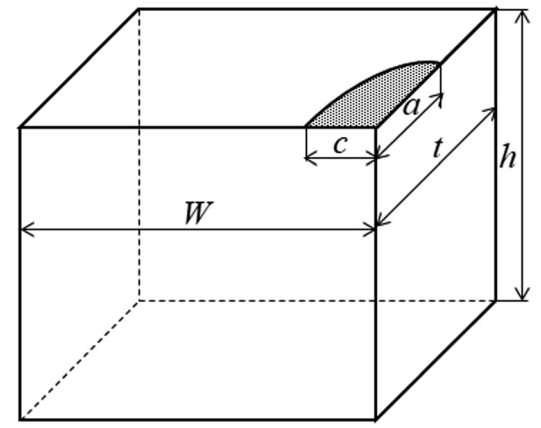

Fig. 2 Analysis model of a semi-elliptical surface crack in a plate

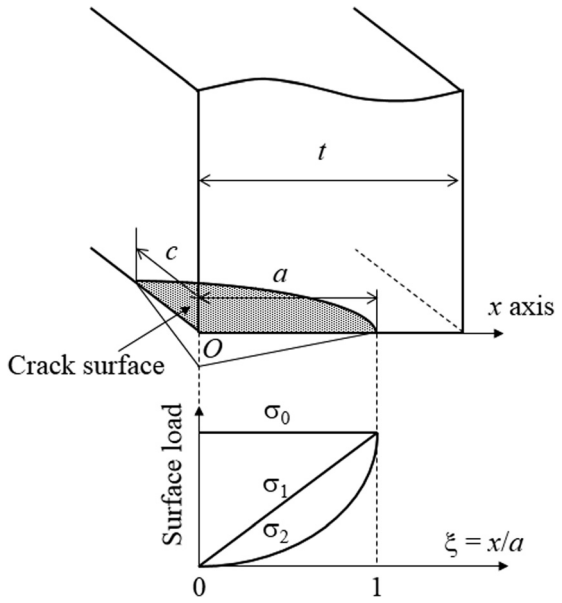

Fig. 3 Stress distribution acting on the crack surface as surface load

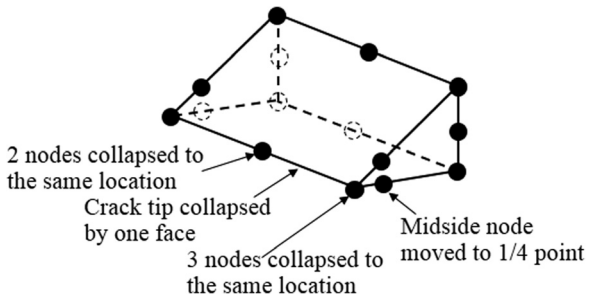

Fig. 4 Singular element used at the crack tip

Table 1 Comparison of applicable ranges of SIF for semi-elliptical surface cracks in plates

Code	Stress distribution	Applicable range of a/ℓ
ASME Section XI	Third-order polynomial	$0.0 \le a/\ell \le 0.5$ for deepest point $0.1 \le a/\ell \le 0.5$ for surface point
JSME FFS		$0.0 \le a/\ell \le 0.5$ for deepest point $0.1 \le a/\ell \le 0.5$ for surface point
API 579-1/ASME FFS-1	Fourth-order polynomial	$0.0 < a/\ell \le 0.5$
RSE-M	Third-order polynomial	$0.0 \le a/\ell \le 0.5$

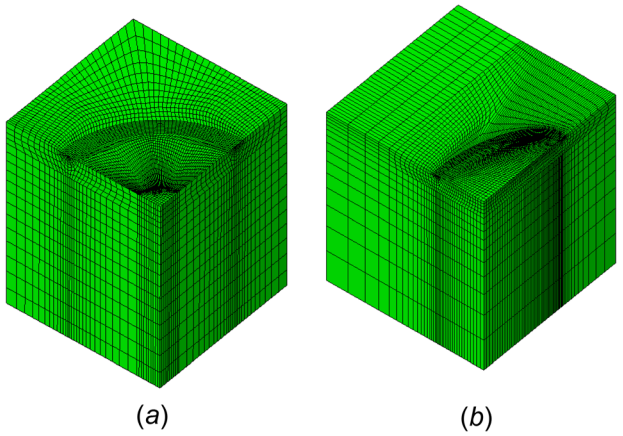

(*a*) (*b*)

Fig. 5 Example meshes near the crack surface for plates with a crack. (*a*) $a/\ell = 0.5$ and $a/t = 0.6$ and (*b*) $a/\ell = 1.0$ and $a/t = 0.6$.

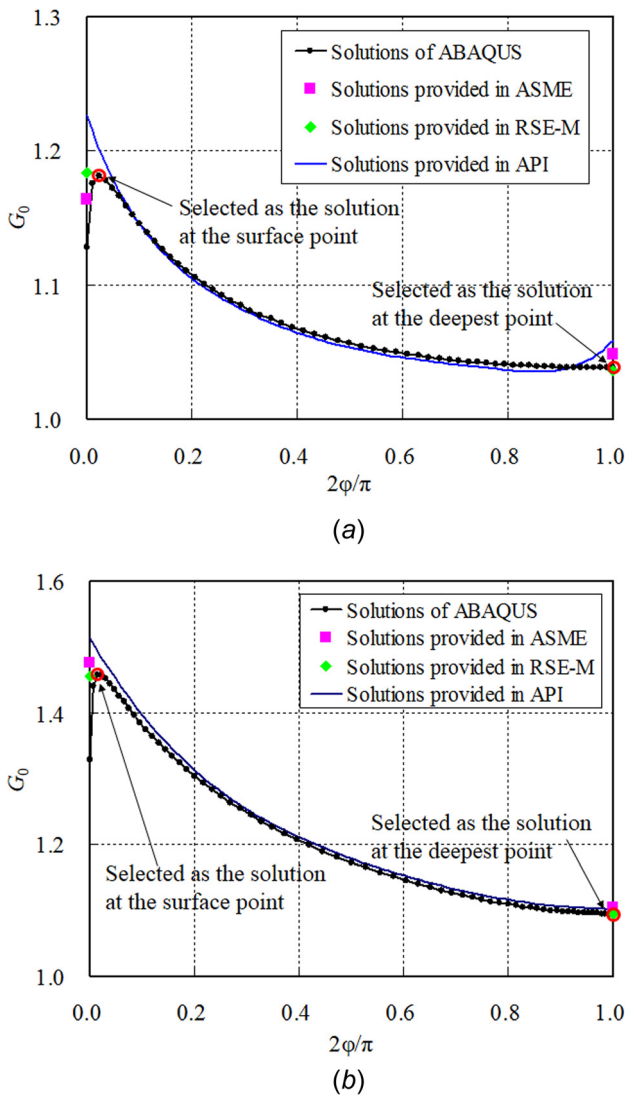

Fig. 6 Relationship between G_0 and the crack front angle for semi-elliptical surface cracks. (*a*) G_0 for crack with $a/\ell = 0.5$ and $a/t = 0.2$ and (*b*) G_0 for crack with $a/\ell = 0.5$ and $a/t = 0.8$.

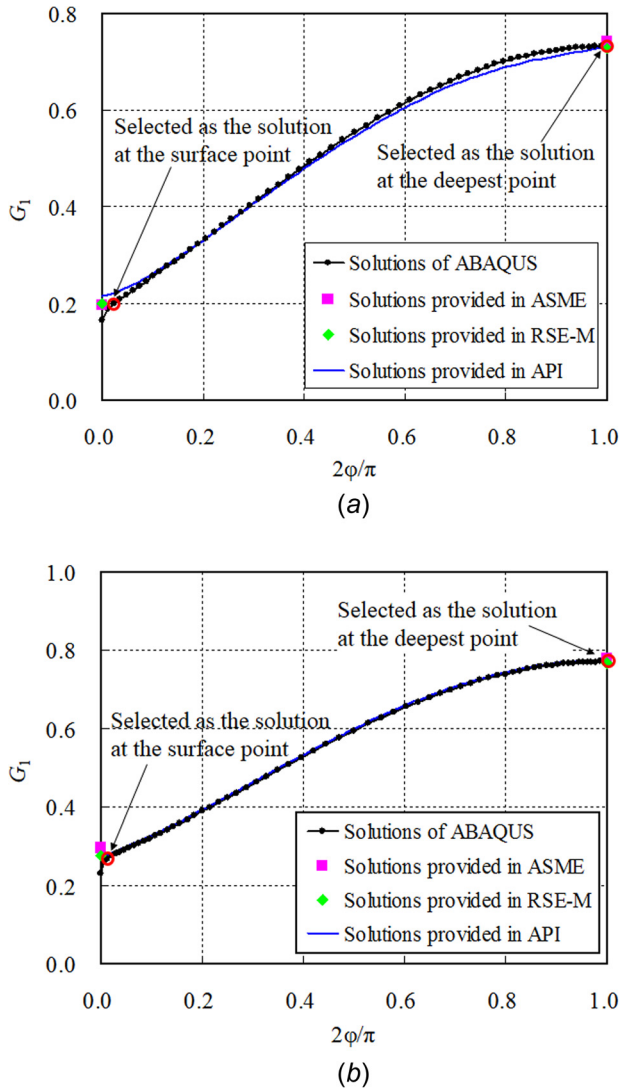

Fig. 7 Relationship between G_1 and the crack front angle for semi-elliptical surface cracks. (*a*) G_1 for crack with $a/\ell = 0.5$ and $a/t = 0.2$ and (*b*) G_1 for crack with $a/\ell = 0.5$ and $a/t = 0.8$.

Therefore, many codes choose to use the SIF solution for $a/\ell = 0.5$, instead of $a/\ell > 0.5$. However, SCC growth is affected by stresses such as weld residual stress and material properties. It is not enough to evaluate SCC using SIF for crack with $a/\ell = 0.5$.

3 Analysis Model

3.1 Expression of SIF. SIF solutions were calculated for semi-elliptical surface cracks with large aspect ratio in plates, using FEA with quadratic hexahedron elements. A fourth-order polynomial equation expressed as follows is used to represent the stress distribution at the crack location:

$$\sigma(x) = A_0 + A_1\left(\frac{x}{a}\right) + A_2\left(\frac{x}{a}\right)^2 + A_3\left(\frac{x}{a}\right)^3 + A_4\left(\frac{x}{a}\right)^4 \quad (1)$$

where a is the crack depth, x is the distance from the surface, and A_0 to A_4 are the coefficients of the fourth-order polynomial stress distribution.

The corresponding SIF solution for the semi-elliptical surface crack is given by

$$K_I = \left[(A_0 + A_p)G_0 + A_1G_1 + A_2G_2 + A_3G_3 + A_4G_4\right]\sqrt{\frac{\pi a}{Q}} \quad (2)$$

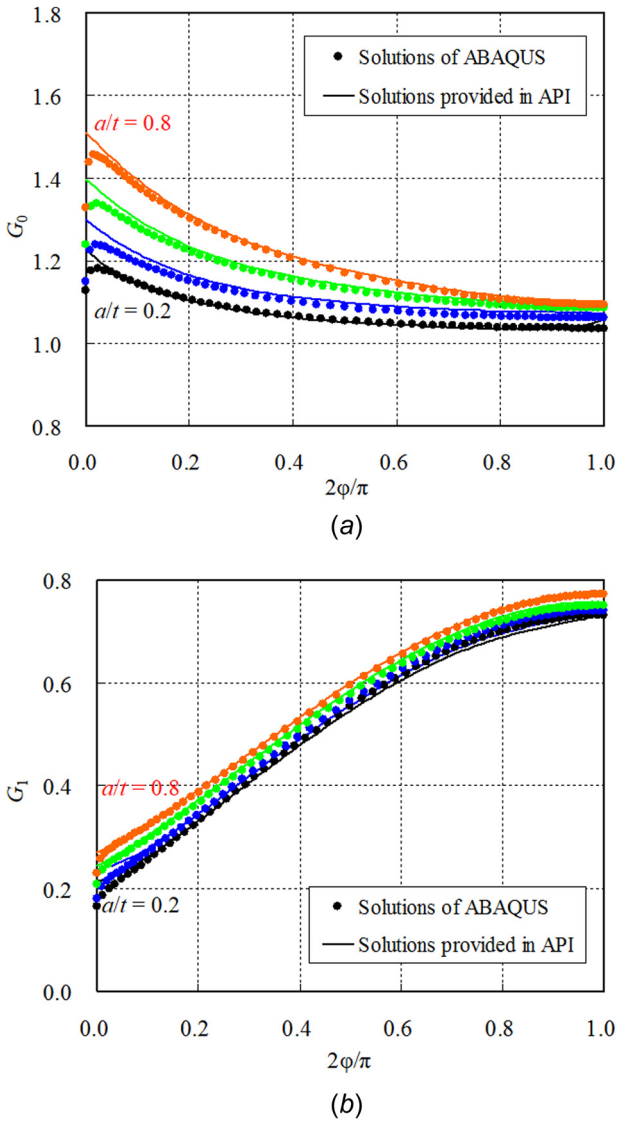

Fig. 8 Relationship between *G* and the crack front angle for cracks with $a/\ell = 0.5$. (*a*) G_0 for cracks with $a/\ell = 0.5$ and (*b*) G_1 for cracks with $a/\ell = 0.5$.

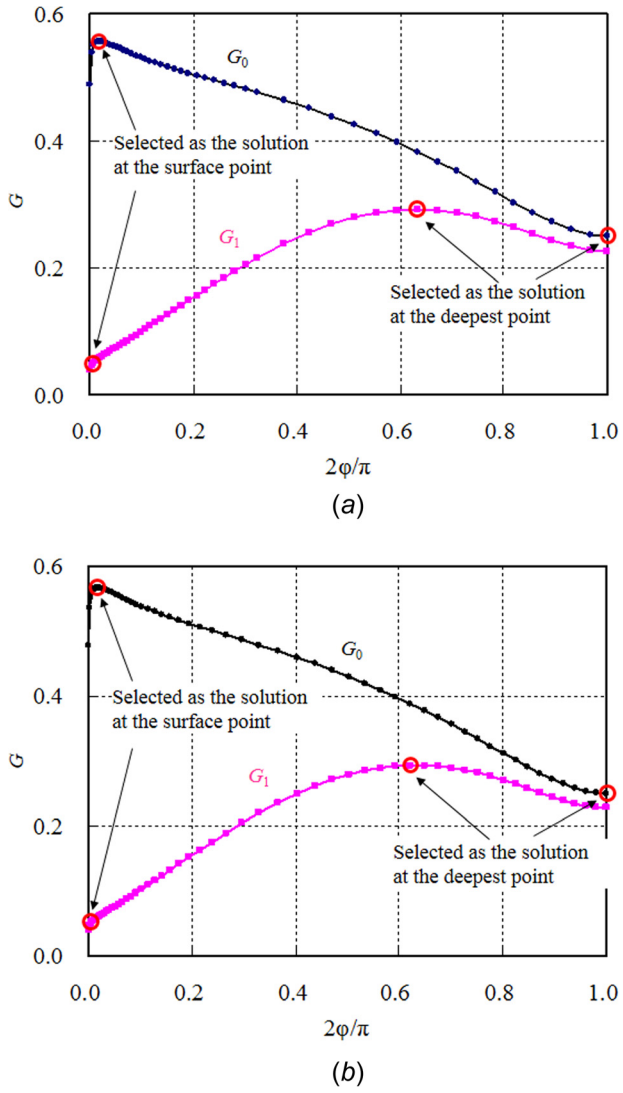

Fig. 9 Relationship between *G* and the crack front angle for cracks with $a/\ell = 2.0$. (*a*) *G* for crack with $a/\ell = 2.0$ and $a/t = 0.4$ and (*b*) *G* for crack with $a/\ell = 2.0$ and $a/t = 0.8$.

where A_p is crack face pressure, G_0 to G_4 are the influence coefficients, and Q is the crack shape parameter. When $a/\ell \le 0.5$, as shown in Fig. 1(*a*), it can be expressed as follows [3–5]:

$$Q = 1.0 + 1.464\left(\frac{a}{c}\right)^{1.65} = 1.0 + 4.593\left(\frac{a}{\ell}\right)^{1.65} \tag{3}$$

where c is the half-length of crack and $\ell = 2c$.

When $a/\ell > 0.5$, as shown in Fig. 1(*b*), Q can be expressed as follows [5]:

$$Q = 1.0 + 1.464\left(\frac{c}{a}\right)^{1.65} = 1.0 + 0.466\left(\frac{\ell}{a}\right)^{1.65} \tag{4}$$

If a fourth-order polynomial equation is used to represent the stress distribution across the entire wall thickness as follows:

$$\sigma(x) = B_0 + B_1\left(\frac{x}{t}\right) + B_2\left(\frac{x}{t}\right)^2 + B_3\left(\frac{x}{t}\right)^3 + B_4\left(\frac{x}{t}\right)^4 \tag{5}$$

It can be transformed into following equation:

$$\sigma(x) = B_0 + B_1\left(\frac{a}{t}\right)\left(\frac{x}{a}\right) + B_2\left(\frac{a}{t}\right)^2\left(\frac{x}{a}\right)^2 + B_3\left(\frac{a}{t}\right)^3\left(\frac{x}{a}\right)^3 + B_4\left(\frac{a}{t}\right)^4\left(\frac{x}{a}\right)^4 \tag{6}$$

where B_0 to B_4 are the coefficients of the polynomial stress distribution across the wall thickness.

The corresponding SIF solution can be obtained by

$$K_I = \left[(B_0 + B_p)G_0 + B_1\left(\frac{a}{t}\right)G_1 + B_2\left(\frac{a}{t}\right)^2 G_2 + B_3\left(\frac{a}{t}\right)^3 G_3 + B_4\left(\frac{a}{t}\right)^4 G_4\right]\sqrt{\frac{\pi a}{Q}} \tag{7}$$

where B_p is crack face pressure.

The SIF solutions analyzed here were investigated along the crack front angle. The definition of the crack front angle φ is also shown in Fig. 1.

3.2 Geometry of Analysis Model. The analysis model is illustrated in Fig. 2 for a semi-elliptical surface crack in a plate. Geometry of the cracks is as follows:

$$a/\ell = 0.5, 1.0, 2.0, \text{ and } 4.0$$

$$a/t = 0.01, 0.1, 0.2, 0.4, 0.6, \text{ and } 0.8$$

In consideration of the structural symmetry, one quarter of the model for the plate was analyzed. The width and height of the plate are $W = h = 50t$ representing an infinite plate. The wall thickness is $t = 30$ mm.

3.3 Stress Acting on the Crack Surface. The stress distribution acting on the crack surface is applied as a distributed surface load as illustrated in Fig. 3 and is expressed as follows:

$$\sigma_i = A_i \left(\frac{x}{a}\right)^i \tag{8}$$

where i is equal to 0–4 for different order of stress distribution, and A_i is the coefficient of the stress distribution corresponding to Eq. (1).

After the SIF solution is calculated through FEA, the influence function shown in Eq. (2) can be obtained using the following relationship:

$$G_i = \frac{K_{\mathrm{I}}^i}{A_i\sqrt{\pi a/Q}} \tag{9}$$

where K_{I}^i is the SIF solution calculated through FEA for the ith-order stress distribution acting on the crack surface.

3.4 FEA Model. The analyses were conducted using ABAQUS Standard 6.9-1 of Dassault Systems Corp. [13]. Twenty-node quadratic hexahedron elements were used. The numbers of elements and nodes are about 120,000 and 500,000, respectively. In order to represent the singularity of the stress distribution at the

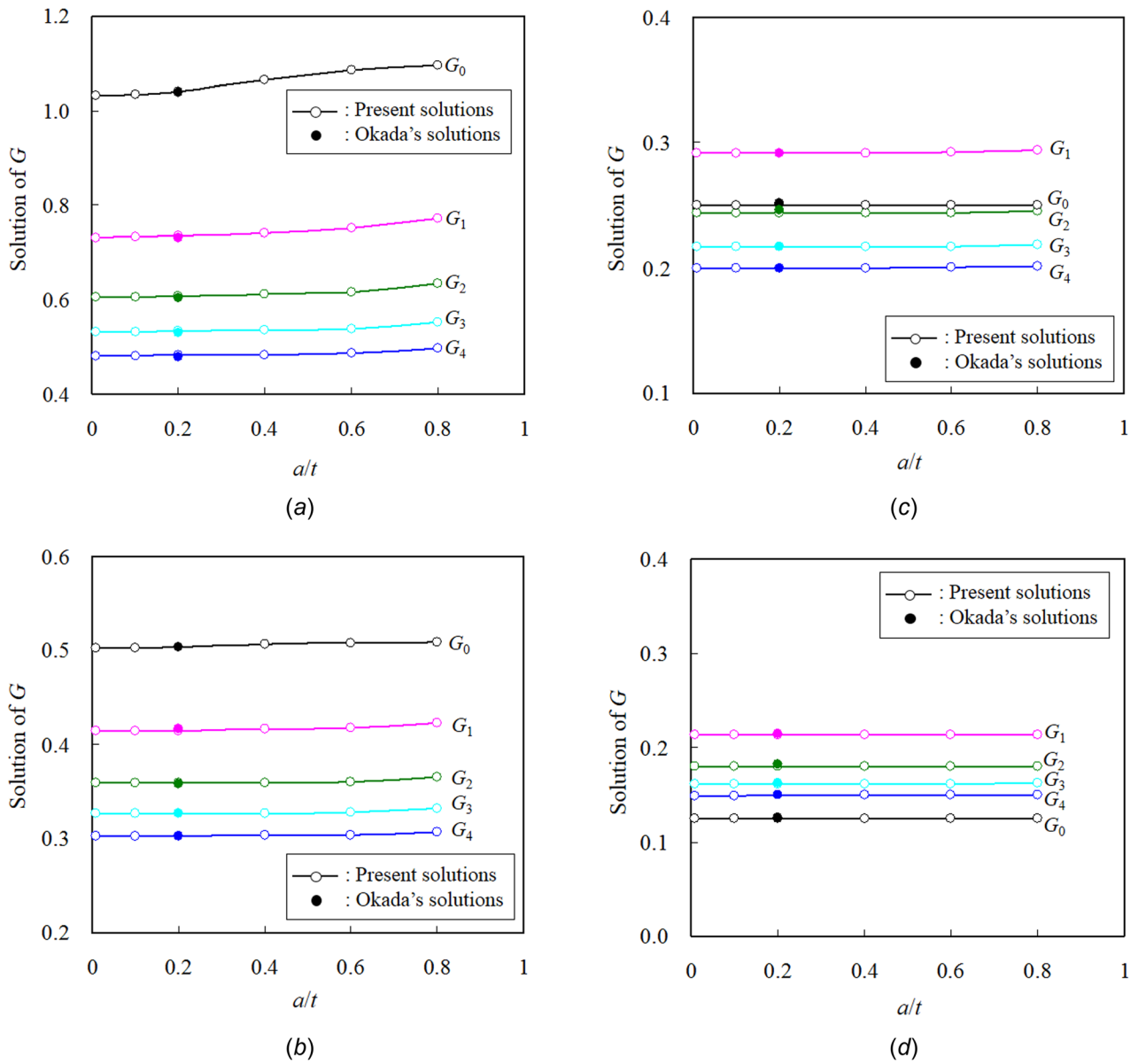

Fig. 10 Results of *G* selected as the solution at the pseudodeepest point of semi-elliptical cracks. (*a*) *G* for cracks with $a/\ell = 0.5$, (*b*) *G* for cracks with $a/\ell = 1.0$, (*c*) *G* for cracks with $a/\ell = 2.0$, and (*d*) *G* for cracks with $a/\ell = 4.0$.

crack tip, one face of the 20-node element connected to the crack tip was collapsed, and the midside node was moved to the 1/4 point nearest the crack tip, as shown in Fig. 4. The example meshes near the crack surface are shown in Fig. 5 for cracks with $a/\ell = 0.5$ and 1.0 for $a/t = 0.6$. Through FEA, the J-integral solutions were obtained for each node along the crack tip. The SIF solutions were derived from the results of the J-integral using the third to fifth J-integral paths. Plane strain condition was assumed when SIF solution was derived from the results of J-integrals. The Young's modulus and Poisson's ratio are $E = 200\,\text{GPa}$ and $\nu = 0.3$, respectively.

4 Numerical Solution and Discussion

4.1 Comparison to Previous Solutions for $a/\ell = 0.5$. As shown in Table 1, the SIF solutions provided in the current codes are applicable to $a/\ell \leq 0.5$. Therefore, in order to check the validity of the influence function solutions obtained in this study, the solutions for cracks with $a/\ell = 0.5$ were compared with the available solutions provided in the current codes. The relationships between the result of G_0 and the crack front angle φ defined in Fig. 1 are shown in Fig. 6 and the relationships between G_1 and φ are shown in Fig. 7, for $a/t = 0.2$ and $a/t = 0.8$. G_2 to G_4 show the same trend as G_1 and thus are omitted in the present paper. The solutions provided in the ASME Section XI, API 579-1/ASME FFS-1, and RSE-M for cracks with $a/\ell = 0.5$ are also shown in Figs. 6 and 7 for comparison.

From an engineering viewpoint, the most important solutions for the semi-elliptical surface cracks are those at the surface point ($\varphi = 0\,\text{deg}$) and the deepest point ($\varphi = 90\,\text{deg}$). It can be seen from Figs. 6 and 7 that, for the cracks with $a/\ell = 0.5$, the FEA results at $\varphi = 90\,\text{deg}$ provided the lowest solution for G_0 and the maximum solution for G_1. Hence, the result from FEA at $\varphi = 90\,\text{deg}$ was selected as the solution of the influence function at the deepest point of the semi-elliptical surface crack. The selected points are illustrated in Figs. 6 and 7. The solutions of the influence functions G_0 to G_4 obtained in this manner are in good agreement with all of the previous provided solutions. The relative difference between them is less than 2%.

It can also be found from Figs. 6 and 7 that there is a narrow singular region near the surface point of the crack. Within this singular region, there is an abrupt drop in the FEA results. Therefore, as an engineering judgment, the FEA result just prior to the abrupt drop was selected as the solution of the influence function at the surface point. No extrapolation was carried out and the selected solution is an actual value obtained from FEA. The selected points are also illustrated in Figs. 6 and 7. The solutions of the influence functions G_0 to G_4 obtained in this manner are in good agreement with the solutions provided in RSE-M. The relative difference between them is less than 3%.

API 579-1/ASME FFS-1 also provided the relationships between the solutions of G_0, G_1, and the crack front angle φ. Therefore, the FEA results were compared with the solutions provided in API 579-1/ASME FFS-1 for cracks with $a/\ell = 0.5$. The relationships between G_0 and the crack front angle φ are shown in Fig. 8(*a*) and the relationships between G_1 and φ are shown in Fig. 8(*b*), for $a/t = 0.2$, 0.4, 0.6, and 0.8. It can be seen from Fig. 8 that the results obtained in this analysis show good agreement with the solutions provided in API 579-1/ASME FFS-1 for general crack front angles apart from the crack surface point, for different ratios of a/t and for both G_0 and G_1. The relative difference for the solution at the deepest point is less than 2%.

4.2 Solution Selection for Cracks With $a/\ell > 0.5$. The SIF solutions obtained in this study for $a/\ell = 0.5$ are in good agreement with those of the ASME Section XI, API 579-1/ASME FFS-1, and RSE-M, as aforementioned. In order to establish the SIF solutions for $a/\ell > 0.5$, the solutions for cracks with $a/\ell = 1.0$, 2.0, and 4.0 were selected from FEA results.

As an example of the FEA results for cracks with $a/\ell > 0.5$, the results of G_0 and G_1 are shown in Fig. 9 as a function of φ, for crack with $a/\ell = 2.0$ and $a/t = 0.4$, 0.8. G_2 to G_4 show the same trend as G_1 and thus are omitted in these figures. It can be seen

Table 2 Solutions at the deepest point of semi-elliptical cracks

			a/ℓ			
G	a/t		0.5	1	2	4
G_0	0.01	Exact	1.0326	0.5025	0.2497	0.1248
		Pseudo	1.0326	0.5025	0.2497	0.1248
	0.1	Exact	1.0338	0.5027	0.2497	0.1248
		Pseudo	1.0338	0.5027	0.2497	0.1248
	0.2	Exact	1.0398	0.5035	0.2498	0.1248
		Pseudo	1.0398	0.5035	0.2498	0.1248
	0.4	Exact	1.0637	0.5064	0.2501	0.1248
		Pseudo	1.0637	0.5064	0.2501	0.1248
	0.6	Exact	1.0862	0.5078	0.2501	0.1248
		Pseudo	1.0862	0.5078	0.2501	0.1248
	0.8	Exact	1.0950	0.5088	0.2501	0.1248
		Pseudo	1.0950	0.5088	0.2501	0.1248
G_1	0.01	Exact	0.7310	0.4072	0.2266	0.1204
		Pseudo	0.7310	0.4147	0.2917	0.2132
	0.1	Exact	0.7314	0.4073	0.2266	0.1204
		Pseudo	0.7314	0.4148	0.2917	0.2132
	0.2	Exact	0.7335	0.4076	0.2267	0.1204
		Pseudo	0.7335	0.4151	0.2918	0.2132
	0.4	Exact	0.7414	0.4085	0.2268	0.1204
		Pseudo	0.7414	0.4162	0.2920	0.2132
	0.6	Exact	0.7502	0.4095	0.2269	0.1204
		Pseudo	0.7502	0.4175	0.2922	0.2133
	0.8	Exact	0.7716	0.4156	0.2282	0.1207
		Pseudo	0.7716	0.4234	0.2937	0.2136
G_2	0.01	Exact	0.6057	0.3588	0.2117	0.1170
		Pseudo	0.6057	0.3588	0.2434	0.1800
	0.1	Exact	0.6059	0.3588	0.2117	0.1170
		Pseudo	0.6059	0.3588	0.2434	0.1800
	0.2	Exact	0.6070	0.3589	0.2117	0.1170
		Pseudo	0.6070	0.3589	0.2434	0.1800
	0.4	Exact	0.6109	0.3594	0.2118	0.1170
		Pseudo	0.6109	0.3594	0.2435	0.1800
	0.6	Exact	0.6158	0.3601	0.2119	0.1170
		Pseudo	0.6158	0.3601	0.2436	0.1801
	0.8	Exact	0.6339	0.3655	0.2131	0.1172
		Pseudo	0.6339	0.3655	0.2449	0.1804
G_3	0.01	Exact	0.5317	0.3267	0.2005	0.1141
		Pseudo	0.5317	0.3267	0.2172	0.1617
	0.1	Exact	0.5318	0.3267	0.2005	0.1141
		Pseudo	0.5318	0.3267	0.2172	0.1617
	0.2	Exact	0.5324	0.3268	0.2005	0.1141
		Pseudo	0.5324	0.3268	0.2172	0.1617
	0.4	Exact	0.5348	0.3271	0.2005	0.1141
		Pseudo	0.5348	0.3271	0.2172	0.1617
	0.6	Exact	0.5380	0.3276	0.2006	0.1141
		Pseudo	0.5380	0.3276	0.2173	0.1618
	0.8	Exact	0.5525	0.3320	0.2016	0.1143
		Pseudo	0.5525	0.3320	0.2184	0.1620
G_4	0.01	Exact	0.4809	0.3030	0.1914	0.1116
		Pseudo	0.4809	0.3030	0.2000	0.1492
	0.1	Exact	0.4810	0.3030	0.1914	0.1116
		Pseudo	0.4810	0.3030	0.2000	0.1492
	0.2	Exact	0.4814	0.3031	0.1914	0.1116
		Pseudo	0.4814	0.3031	0.2000	0.1492
	0.4	Exact	0.4829	0.3033	0.1914	0.1116
		Pseudo	0.4829	0.3033	0.2001	0.1492
	0.6	Exact	0.4852	0.3036	0.1915	0.1116
		Pseudo	0.4852	0.3036	0.2001	0.1492
	0.8	Exact	0.4969	0.3072	0.1923	0.1117
		Pseudo	0.4969	0.3072	0.2010	0.1494

Note: For each a/t value, the upper row represents the G value at the exact deepest point, and the lower row represents the value conservatively selected for the deepest point.

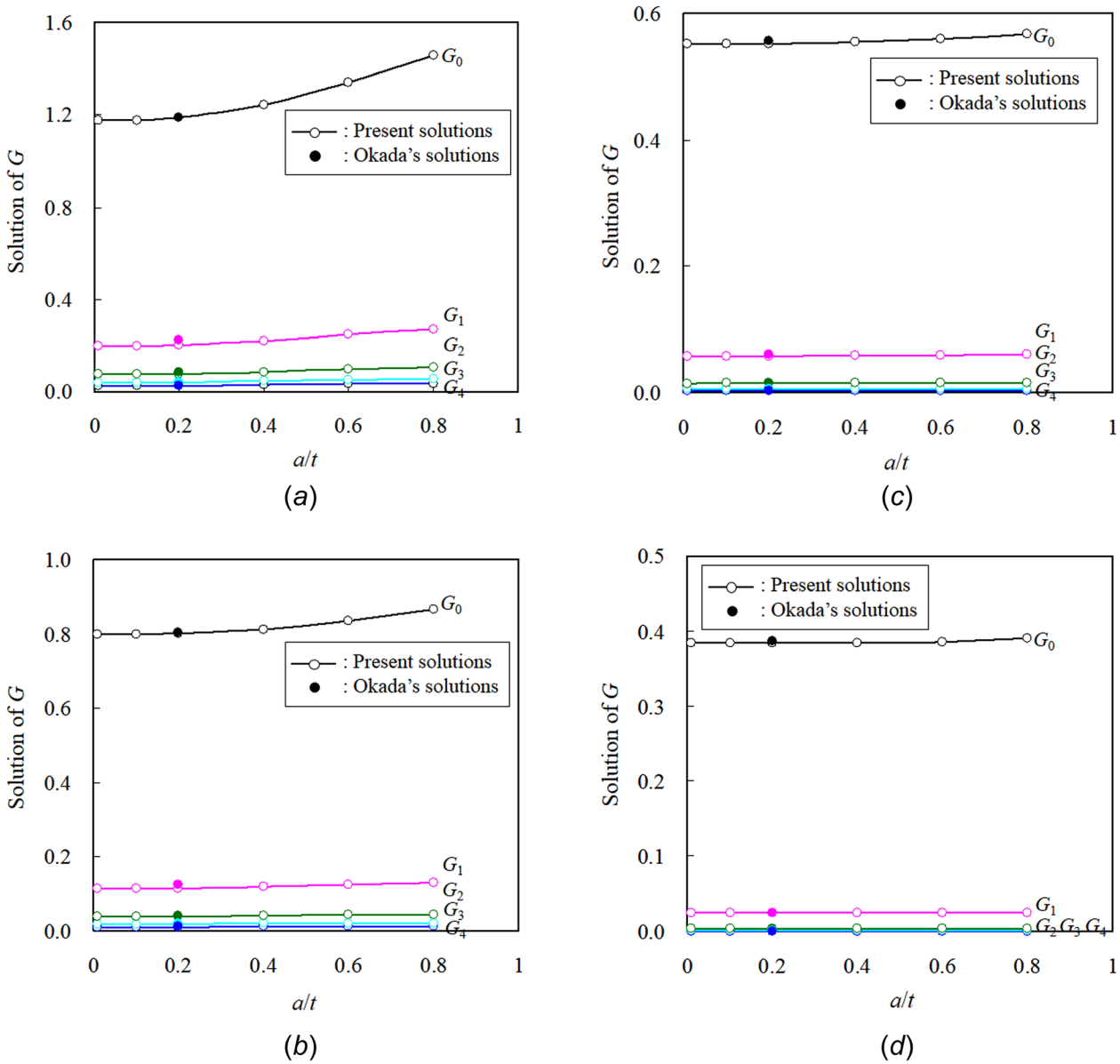

Fig. 11 Results of *G* selected as the solution at the surface point of semi-elliptical cracks. (*a*) *G* for cracks with $a/\ell = 0.5$, (*b*) *G* for cracks with $a/\ell = 1.0$, (*c*) *G* for cracks with $a/\ell = 2.0$, and (*d*) *G* for cracks with $a/\ell = 4.0$.

from Fig. 9 that the maximum result of G_1 appears at neither the exact deepest point nor the surface point of the crack; it appears at the halfway point of the crack front. This phenomenon was also reported for surface cracks with large aspect ratio in Ref. [8]. In this study, the maximum FEA results for G_1 to G_4 along the crack front were selected as the SIF solutions at the deepest point for cracks with $a/\ell > 0.5$ for conservative estimation. The selected points are shown in Fig. 9. These selected points are named as the pseudo deepest points and the points at $\varphi = 90$ deg are called the exact deepest points hereafter.

For the solution of G_0 at the deepest point and the solutions of G_0 to G_4 at the surface point of the crack, the selected points of the FEA result are the same as that illustrated in Figs. 6 and 7. The selected points are also illustrated in Fig. 9.

4.3 Solutions of SIF. Corresponding to the investigation described above, the results of the influence function selected as the deepest point solutions of cracks are shown in Fig. 10 as open circles and lines. The values are summarized in Table 2. In the table, the direct results at the exact deepest point, that is the location of $\varphi = 90$ deg, are also provided as a reference. The results of the influence function which were selected as the surface point solutions of cracks are shown in Fig. 11 and the values are summarized in Table 3. For comparison, the solutions of G_0 to G_3 obtained by Okada et al. [12] are also included in Figs. 10 and 11 as solid circles, for $a/t = 0.2$. Their solutions were obtained using FEA with quadratic tetrahedral elements and the VCCM method, as described above.

It can be seen from Figs. 10 and 11, the influence function solutions obtained in this study using FEA with quadratic hexahedron elements are in good agreement with the solutions obtained by Okada at $a/t = 0.2$. It can also be seen from Figs. 10 and 11, when $a/\ell = 0.5$, the solutions of the influence function increase with the increase in a/t. On the other hand, when $a/\ell > 0.5$, the increasing trend of the influence function becomes insensitive with regard to the increase in a/t. It can also be seen from Fig. 11, for the influence function solution at the surface point, the solutions of G_1 to G_4 are significantly small compared to G_0.

Table 3 Solutions at the surface point of semi-elliptical cracks

		a/ℓ			
G	a/t	0.5	1	2	4
G_0	0.01	1.1753	0.7988	0.5518	0.3841
	0.1	1.1770	0.7991	0.5519	0.3841
	0.2	1.1865	0.8012	0.5523	0.3842
	0.4	1.2413	0.8132	0.5546	0.3846
	0.6	1.3397	0.8353	0.5591	0.3854
	0.8	1.4571	0.8676	0.5670	0.3904
G_1	0.01	0.1966	0.1145	0.0575	0.0245
	0.1	0.1972	0.1146	0.0575	0.0246
	0.2	0.2004	0.1153	0.0576	0.0246
	0.4	0.2181	0.1191	0.0583	0.0247
	0.6	0.2469	0.1250	0.0594	0.0249
	0.8	0.2684	0.1308	0.0603	0.0249
G_2	0.01	0.0735	0.0386	0.0148	0.0041
	0.1	0.0738	0.0386	0.0148	0.0041
	0.2	0.0755	0.0390	0.0148	0.0041
	0.4	0.0841	0.0408	0.0152	0.0042
	0.6	0.0971	0.0433	0.0156	0.0042
	0.8	0.1052	0.0445	0.0156	0.0042
G_3	0.01	0.0383	0.0187	0.0060	0.0012
	0.1	0.0385	0.0188	0.0060	0.0012
	0.2	0.0395	0.0190	0.0060	0.0012
	0.4	0.0445	0.0200	0.0062	0.0012
	0.6	0.0517	0.0213	0.0064	0.0013
	0.8	0.0550	0.0214	0.0064	0.0013
G_4	0.01	0.0234	0.0109	0.0031	0.0005
	0.1	0.0236	0.0110	0.0031	0.0005
	0.2	0.0242	0.0111	0.0031	0.0005
	0.4	0.0276	0.0118	0.0032	0.0005
	0.6	0.0320	0.0125	0.0033	0.0005
	0.8	0.0333	0.0125	0.0033	0.0005

5 Summary and Conclusions

Since SCCs were detected in nuclear components, SIF solutions for surface cracks with large aspect ratio were required to perform an integrity assessment. In this study, the authors developed the SIF solutions using FEA with quadratic hexahedron elements for semi-elliptical surface cracks with a wide range of large aspect ratios in plates. The SIF solutions for cracks with $a/\ell = 0.5$ are provided in the current codes such as the ASME Section XI, API 579-1/ASME FFS-1, or RSE-M. Nearly, identical values were obtained from FEA. Based on the investigation for cracks with $a/\ell = 0.5$, SIF solutions for large aspect ratios with $a/\ell = 1.0$, 2.0, and 4.0 were calculated for different crack depths of $a/t = 0.01$–0.8. The developed SIF solutions were coincident with those by VCCM method for the case of $a/t = 0.2$. Therefore, it should be emphasized that the SIF solutions developed in this paper for cracks with $a/\ell \geq 0.5$ and $a/t = 0.01$–0.8 are pertinent to evaluation of subcritical crack growth behavior. In addition, SIF solutions are summarized as tabulation toward codification.

Acknowledgment

The authors wish to thank the chairs and members of the ASME Section XI Working Groups on Pipe Flaw Evaluation and Flaw Evaluation for their supports and suggestions.

References

[1] Nakamura, T., Taniguchi, K., Hirano, S., Marekazu, N., and Sato, T., 2009, "Stress Corrosion Cracking in Welds of Reactor Vessel Nozzle at Ohi-3 and of Other Vessel's Nozzle at Japan's PWR Plants," ASME Paper No. PVP2009-77344.

[2] Hatamura Institute for the Advancement of Technology: Failure Knowledge Database, http://www.sozogaku.com/fkd/cf/CB0041003.html (in Japanese)

[3] ASME, 2013, *ASME B&PV Code Section XI, Rules for Inservice Inspection of Nuclear Power Plant Components*, ASME, New York.

[4] JSME, 2012, *Rules on Fitness-for-Service for Nuclear Power Plants*, The Japan Society of Mechanical Engineers, Tokyo, Japan.

[5] API/ASME, 2007, *Recommended Practice for Fitness-for-Service*, American Petroleum Institute and the American Society of Mechanical Engineers, API 579-1/ASME FFS-1. Available at: https://www.asme.org/products/courses/api-5791asme-ffs1-fitness-service

[6] Marie, S., Chapuliot, S., Kayser, Y., Lacire, M. H., Drubaya, B., Bartheletc, B., Le Dellioud, P., Rougiere, V., Naudinf, C., Gillesg, P., and Triayg, M., 2007, "French RSE-M and RCC-MR Code Appendices for Flaw Analysis: Presentation of the Fracture Parameters Calculation—Part III: Cracked Pipes," Int. J. Pressure Vessels Piping, **84**(10–11), pp. 614–658.

[7] Rudland, D., Shim, D.-J., and Xu, S., 2013, "Simulating Natural Axial Crack Growth in Dissimilar Metal Welds Due to Primary Water Stress Corrosion Cracking," ASME Paper No. PVP2013-97188.

[8] Malekian, C., Wyart, E., Savelsberg, M., Teughels, A., Fouquet, P.-E., Minjauw, N., and Wendling, A., 2009, "Stress Intensity Factors for Semi-Elliptical Surface Cracks With Flaw Aspect Ratio Beyond the ASME XI Limit," ASME Paper No. PVP2009-77917.

[9] Iwamatsu, F., Miyazaki, K., and Shiratori, M., 2011, "Development of Evaluation Method of Stress Intensity Factor and Fatigue Crack Growth Behavior of Surface Crack Under Arbitrarily Stress Distribution by Using Influence Function Method," Trans. Jpn. Soc. Mech. Eng., Ser. A, **77**(782), pp. 1613–1624.

[10] Ochi, M., Hojo, K., Ogawa, K., and Ogawa, N., 2009, "Simplified Stress Intensity Factor Equation for SCC Propagation in the Pipe Welds (Step 2)," ASME Paper No. PVP2009-78001.

[11] Okada, H., Kawai, H., and Araki, K., 2008, "A Virtual Crack Closure-Integral Method (VCCM) to Compute the Energy Release Rates and Stress Intensity Factors Based on Quadratic Tetrahedral Finite Elements," Eng. Fract. Mech., **75**(15), pp. 4466–4485.

[12] Okada, H., Koya, H., Kawai, H., and Li, Y., 2012, "Computations of Stress Intensity Factors for Deep Cracks in Plates by Using the Tetrahedral Finite Element," ASME Paper No. PVP2012-78580.

[13] ABAQUS 6.9-1, Dassault Simulia, 2009.